Chapter 5

Effects of Photonic Crystal Band Gap on Rotation and Deformation of Hollow Te Rods in Triangular Lattice

In chapter 3 and 4, we have demonstrated that the deformed rods, rotational rods and perturbation of shape of rods strongly affect the band structures of 2D photonic crystals. The solid rods are used for a given lattice type, and the rotational and structural symmetries influencing the band structures have been examined systematically. The results may provide guiding routes for fabrication and design the photonic crystals. Recently, the hollow oval rods have been designed as inclusions in the triangular lattice.[66,67] The anisotropic materials are used, and the results have shown that photonic crystal exhibit a large PBG at high normalized frequencies. The importance of hollow structure in the photonic crystal can be understood from the viewpoints of fabricated process and structural design. It's known that the standard fabrication of 2D PCs is the electrochemical etching of rods in a slab of materials. The etching process may result in a rough and porous interface between the rods and the background matrix. This interface can be described by an effective medium, and its dielectric constant may be different. The thickness and dielectric constant of interfacial layers are dependent on the preparation process of the PCs, and the interfacial layer influencing the properties of band structures can be calculated and realized by using hollow structure as inclusions in the photonic crystal.

The dependence of band structures on the shape of hollow rods are more

complicated than that on the shape of solid rod, the high-frequency bands especially. The hollow part of rods is equivalent to a cavity, and the propagation of light of high frequency in the hollow rods may depend strongly on the shape of rod. The study of high-frequency band gaps is an important topic for fabricating a large size of photonic device. The hollow structure may provide a possible method to realize a large PBG in high frequency region. Some studies have focused on the design of hollow oval structure, such as geometric parameters, dielectric constant, for obtaining a large complete PBG.[67] However, the effects of structural and rotational symmetries associated with the deformation and rotation of rods on E-polarization and H-polarization band gaps of the system has not been studied thoroughly.

This work investigates the effect of structural and rotational symmetries on the E-polarization and H-polarization band gaps of hollow rods embedded in a triangular lattice. The plane-wave method is employed to calculate the band structures and field patterns. The symmetry of hollow rods is more complex than that of solid rods because the former can be broken by deforming and rotating inner and shell rods. Three deformed and two rotational structures are constructed in this study. Three deformed structures, involving inner-rod deformation, shell-rod deformation and whole-rod deformation, are considered to explore the effect of structural deformation on the band structures. Two rotational structures -inner rod rotation and whole rod rotation- are introduced to investigate the effect of rotational symmetry on the band structures. The correlations between the hollow structures and PBGs can be reasonably explained, and the scattering mechanisms are systematically examined.

5.1. Dielectric Function of Hollow Structure

Figure 5.1 displays the geometry of the 2D triangular lattice of hollow oval rods,

where a is the lattice constant, $\bar{a}_1 = a(1,0)$ and $\bar{a}_2 = a(1/2, \sqrt{3}/2)$ are the basic vectors of the triangular lattice. Each hollow rod comprises an inner rod (hollow portion) with isotropic dielectric constant ε_r, and an outer shell with anisotropic dielectric constants ε_e and ε_o. The optical property of anisotropic material is described in Fig. 5.2. The structured background is homogeneous with dielectric constant ε_b. The dimensions of the inner rod and the outer shell are, in units of lattice constant a and in the directions of the major and minor axes, (ℓ_1, w_1) and (ℓ_2, w_2), respectively. The terms $\alpha_1 = \ell_1 / w_1$ and $\alpha_2 = \ell_2 / w_2$ are used for convenience.

The plane-wave theory and method have been described in chapter two. The electromagnetic fields in the 2D photonic crystals are obtained by solving master equation. Here only the dielectric function of hollow structure is expressed. As shown in Fig. 5.3, the dielectric constant can be written as,

$$\varepsilon(\vec{r}) = \varepsilon_b + (\varepsilon_{e,o} - \varepsilon_b) S_{shell}(\vec{r}) + (\varepsilon_r - \varepsilon_b) S_{inner}(\vec{r}) \tag{5.1}$$

where $S_{shell}(\vec{r})$ and $S_{rod}(\vec{r})$ are the functions of the outer shell and the inner rod, respectively. The magnitudes of these two functions are set to unity inside the interesting region and zero outside. The Fourier transform of $\varepsilon(\vec{r})$ is,

$$\begin{aligned} \varepsilon(\vec{G}) = {} & \varepsilon_b \delta_{G,0} + (\varepsilon_{e,o} - \varepsilon_b) \frac{2 f_{shell}}{\sqrt{g_2(\theta_2)}\ell_2} J_1(\sqrt{g_2(\theta_2)}\ell_2) \\ & + (\varepsilon_r - \varepsilon_b) \frac{2 f_{rod}}{\sqrt{g_1(\theta_1)}\ell_1} J_1(\sqrt{g_1(\theta_1)}\ell_1) \end{aligned} \tag{5.2}$$

The second and third terms represent $\varepsilon(\vec{G})$ for the shell and the inner rods, respectively. The factors $f_{shell} = (\pi \ell_2 w_2)/A_{cell}$ and $f_{rod} = (\pi \ell_1 w_1)/A_{cell}$ are the ratios of the area of the outer shell and of the inner rod to the area of a primitive unit cell. J_1 is the Bessel function of the first kind. The function $g_1(\theta_1)$ represents the magnitude of the reciprocal-lattice vector as inner rods are rotated through an angle θ_1, and the function $g_2(\theta_2)$ represents the magnitude of the reciprocal-lattice vector as the outer

shells are rotated through an angle θ_2. They are given by

$$g_{1,2}(\theta) = G_x^2(\cos^2\theta_{1,2} + \alpha_{1,2}{}^{-2}\sin^2\theta_{1,2}) + G_y^2(\sin^2\theta_{1,2} + \alpha_{1,2}{}^{-2}\cos^2\theta_{1,2}) + 2G_xG_y\sin\theta_{1,2}\cos\theta_{1,2}(1-\alpha_{1,2}{}^{-2}) \quad (5.3)$$

where G_x and G_y are the x- and y-axial components of $\vec{G}$, respectively. The band structures for such anisotropic photonic crystals can be calculated in the same way as for isotropic crystals. In this study, 1000 plane waves were adopted, and the computational errors in the E- and H-polarization modes for each case were estimated to be less than 1%.

5.2. Effect of Deformed Symmetry of Hollow Structure on Band Structures

This study calculates photonic-band structures of hollow Te (tellurium) rods in a triangular lattice. The hollow rods with cross section in the size of micrometers could be patterned with the nano-lithographic technology. However, Te is not the popular material for the current lithographic technology; it is still not well developed for making Te microstructures to photonic crystals. The usage of Te in this study is taking advantage of its high refractive index. The high index of refractivity allows us to tune the complete PBG within a large extent. Furthermore, the large difference between the extraordinary and the ordinary refractive indices also permits us to study more flexibly about the effects of the structural and rotational symmetries on the PBG of hollow structure.

In this study, we calculated the photonic band structures of Te shells, which possess the anisotropic optical properties with refractive indices $n_e = 6.2$ and $n_o = 4.8$. The dielectric constants for the background material and the inner hole portion are taken as $\varepsilon_b = \varepsilon_r = 1$. Figure 5.4 shows the band structure for a triangular

lattice of hollow oval rods at a rotation angle of $\theta_1 = \theta_2 = 0°$. The geometric parameters (ℓ_1, ℓ_2, α) for hollow oval rods are taken as $\ell_1 = 0.27a$, $\ell_2 = 0.48a$, and $\alpha = 1.58$. The solid curves are for the H-polarization modes and the dotted curves are for the E-polarization modes. It has to be noted that k-lines Γ-M-K-Γ of 1/12 of the irreducible Brillouin zone may be not sufficient to identify the minimum complete PBG for an arbitrarily deformed or rotational hollow rods, because of the breakdown of symmetry laws. All modes throughout the calculations are plotted along the M-K-Γ-M'-K'-M path in the first Brillouin zone. From the figure, one can see that there are three complete PBGs for this photonic crystal structure and the gap widths are about 0.009, 0.052, and 0.041$(wa/2\pi c)$. Note, especially for the E-polarization modes, that the band structure has not only many discrete band gaps but also a flat-band property near the complete PBG edge.

For Te, its extraordinary refractive index and ordinary refractive index of actually decrease with optical wavelength λ from $(n_e = 6.372, n_o = 4.929)$ at λ = 3.5 μm to $(n_e = 6.23, n_o = 4.785)$ at λ = 14 μm.[63,67,68] To verify the validity of calculated photonic band structures with assumed constant refractive indices, we calculated the photonic band structures of a hollow oval Te rod photonic crystal with various refractive indices which are constant with frequency. Table 1 lists the widths of first two complete PBG of an A-type photonic crystal considered in this study with various minor changed refractive index sets (n_e, n_o) in the range between (6.18, 4.78) and (6.22, 4.82). The width of the first complete PBG remains almost unchanged for a constant n_e with varying n_o and varies about 2.5% within the set range. The result can be interpreted alternatively that for a photonic crystal with refractive indices varying with frequency in the range between (6.18, 4.78) and (6.22, 4.82), its first complete PBG width will

deviate most 2.5% [=(0.052-0.0507)/0.052] from the averaged first complete PBG widths which are accounted to the non-wavelength dependent refractive indices in the set range. That is, the calculated gap width accordingly is inherently involved 2.5% inaccuracy, which is nevertheless acceptable as being a base for analysis, compared with exact solution for refractive indices being varying with frequency. Comparatively, the width of the second complete PBG associated with the high-order modes appears disordered without a significant trend. For the large width variation, the apriority for the first complete PBG width cannot be plausibly applied to the case for the second complete PBG width. Accordingly, the use of the constant refractive indices for calculations is reasonable in suitable infrared regime. In this work, Te has anisotropic optical properties with approximate extraordinary refractive index $n_e = 6.2$ and ordinary refractive index $n_o = 4.8$ in the wavelength regime between 3.5 and 14 μm.

The absorption coefficient of Te in the infrared region is less than 1 cm^{-1}.[69] In the appropriate infrared range and for a photonic crystal with limited size, the refractive indices of Te can be treated as constants and the absorption effect can be neglected in the calculation. In fact, a preliminary calculation shows that very small uncertainty involved in our calculation when the refractive indices of Te is assumed as constants and the absorption effect is neglected. The axis of Te rod is set to be parallel to the extraordinary axis and provides different refractive indices for the E- and H-polarization modes in the structure. The band gaps of two modes are overlapped to give the complete PBG width of the photonic crystal system.

The dielectric constants of the background material and the inner holes are set to $\varepsilon_b = \varepsilon_r = 1$. Three deformed structures, A, B and C are considered to investigate the effect of the shape of a hollow rod on the PBG. The schematic diagram for three deformed structures is displayed in Fig. 5.5. The structures are deformed by altering the factors α_1 and α_2, which are designed to prevent overlap between nearest

neighboring rods. The optimal parameters of major axes of inner rods and outer shells, taking as $\ell_1 = 0.27a$ and $\ell_2 = 0.48a$, are adopted throughout the simulation to study how the structural and rotational symmetries affect the PBG of hollow structure. Basically, the choice of $\ell_1 = 0.27a$ and $\ell_2 = 0.48a$ provides us eclectically the largest two complete PBG widths. And both complete PBG widths decrease with increasing ℓ_2 for a constant ℓ_1 but fluctuate with varying ℓ_1 for a constant ℓ_2. Table 2 lists the widths of first two complete PBG, in unit of $\omega a/2\pi c$, of A-type photonic crystals considered in this study with constant refractive indices $(n_e = 6.2, n_o = 4.8)$ and various *L*1 and L2 lengths. Basically, the photonic crystal with L1 = 0.27a and L2 = 0.48a (a is lattice constant.) provides eclectically the largest two complete PBG widths. Roughly, both complete PBG widths decrease with increasing L2 for a constant L1 but fluctuate with varying L1 for a constant L2.

Structures A are designed such that the lengths of the minor axes of the inner and shell rods are simultaneously reduced to equalize α_1 and α_2. Figure 5.6(a) presents the dependence of the gap map on α_1. Many gaps appear for E-polarization modes, and three gaps appear for H-polarization modes between 0.2 and 0.8$(\omega a/2\pi c)$. The width of the H1 gap is maximal at $\alpha_1 = 1$, and is zero at approximately $\alpha_1 = 1.7$. H2 and H3 gaps do not appear in the hollow circular structure, until structural symmetry is broken. As shown in the diagram, this configuration generally has three complete PBGs and the E-polarization modes dominate the complete PBG widths.

Structures B with circular inner rods ($\alpha_1 = 1$) and vertically deformed shell rods are considered. That is, the structural symmetry of the inner rod is retained, whereas that of the shell rod is broken. Figure 5.6 (b) presents the calculations. When α_2 exceeds 1.35, the gap widths of the E-polarization modes vary more than those in structures A, drastically reducing the complete gap widths. However, the width of the H-polarization

gap as a function of α_2 is quite similar to those in structures A. The width of the H1 gap declines while that of the H3 gap increases as α_2 increases. The behavior of the H3 gap width can be elucidated by wave scattering in the hollow rods. The propagation of light of short wavelength in the hollow rods depends strongly on the shape of rod, so resonance can be easily produced. Therefore, the shape of the rod determines the high-frequency gaps of H-polarization modes. With respect to the H1 gap, light with long wavelength cannot easily be trapped with resonance in the rods, so the interaction among the fields of the rods must be examined in detail. In the H-polarization modes, fields are oriented in the x-y plane and the tangential fields that connect nearest-neighboring rods must be forced to penetrate regions of air to satisfy the continuity boundary condition. Accordingly, the variation in the y-directional length influences the fraction of energy in the dielectric regions, and thereby alters the low-frequency gap width.

Structures C have circular shell rods ($\alpha_2 = 1$) and deformed inner rods. The air-space sizes between the rods are very thin in such structures. As shown in Fig. 5.6 (c), the width of the H1 gap is almost independent of α_1, because the air-space sizes among the rods are kept invariable, while the width of the H3 gap varies drastically, since the rods are deformed. Furthermore, the width of the E-polarization gap may not be increased by reducing the structural symmetry of the inner rods, so no complete PBG is present in such structures.

The calculated band gaps of structures A, B and C show that the E-polarization modes dominate the complete PBG widths. The field patterns of each structure are examined to investigate the effect of structural symmetry on the E-polarization modes. Figures 5.7(a)-(d) show the level distribution of the displacement field in hollow circular structures and deformed structures A, B and C, respectively. Each figure plots the distribution of magnitudes of the displacement field associated with the seventh

band at the *K*-symmetry point. The fields in structure A are concentrated in the dielectric regions for all $\alpha_1(=\alpha_2)$ values. However, the deformation in the shell rods of structure B strongly influences the field distribution. In particular, the displacement fields in the thin section are expelled from the dielectric region and are distributed non-uniformly within the rods, so the gap widths in the E-polarization modes of structure B vary more than those of structure A. Figure 5.7(d) shows the field patterns in structure C. The variation in the field distribution is not as strong as that in structure B as the geometry of the rods is changed. This result may be attributed to the fact that the sizes of the inner rods are not large enough and the field distribution is similar to that in the hollow circular structure.

5.3. Effect of Rotational Symmetry of Hollow Oval Structure on Band Structures

The symmetry of the hollow structure can also be broken by rotating the inner and shell parts without changing the geometric parameters. Figure 5.8(a) and (b) show the representation of inner and whole rod rotation, respectively. Two rotations, inner and whole rod rotation, under the geometric parameter constant $\alpha_1 = \alpha_2$, are considered herein. All structures have the same filling fraction but are differently orientated with respect to the triangular lattice. Figures 5.9(a) and (b) show the photonic band structures associated with rotations of the inner and whole rods, respectively, through an angle of 30°. The geometric parameters (ℓ_1, ℓ_2, α) for hollow oval rods are taken as $\ell_1 = 0.27a$, $\ell_2 = 0.48a$, and $\alpha = 1.6$. The line shapes of the H-polarization bands of the inner-rod rotation are identical to those in Fig. 5.4, but they shift simultaneously downward in frequency. The H-polarization band structures also exhibit the same tendency at an arbitrary angle of rotation θ_1. However, the line

shapes of the H-polarization bands associated with the rotation of the whole rod vary more than those in Fig. 5.4. The reason for the difference between band structures associated with inner and whole rod rotations can be elucidated by considering eq. 5.2. On the basis of the assumption that the inner rods of each rotational type are rotated through the same angle, the third terms for both rotational types are equal. However, the shell orientation associated with the whole rotation differs from that associated with the inner rotation, and $\sqrt{g(\theta)}$ in the second term dominates the difference between the band structures of the inner-rod and whole-rod rotations.

Figures 5.10(a) and (b) plot the H-polarization gap width against the angles of inner-rod and whole-rod rotations, respectively. The rotational symmetry of each structure is such that a $90°$ angular period of the gap width is obtained for the inner-rod rotation, and a $60°$ angular period of the gap width is obtained for the whole-rod rotation. For the inner-rod rotation, the width of the third gap (H3) increases to 150% at a rotation angle of $\theta_1 = 90°$, while the widths of the first gap (H1) and the second gap (H2) decline markedly as the angle of rotation increases. For the whole-rod rotation, the H1 gap width increases to reach a maximum gap width at a rotation angle of $\theta_1 = \theta_2 = 30°$, while the H3 gap width approaches zero at around $\theta_1 = \theta_2 = 40°$. Furthermore, the dependence of the H1 and H3 gap widths on rotating angle for various α have also been examined.

Figures 5.11(a) and (b) show the H1 gap widths associated with inner and whole rod rotations for various α_1. The width of the H1 gap slightly decreases under the inner-rod rotation as the angle of rotation increases. Notably, the air-space sizes among the rods remain constant under the inner-rod rotation through an arbitrary angle, indicating that the interaction between the fields of the rods affects the H-polarization modes almost equally at any angle of rotation. At whole-rod rotation

drastically increases the width of the H1 gap; the gap width is largest at approximately $\theta_1 = 30^\circ$. These results are attributable to the strong interactions among the rods and the reduction in the rotational symmetry. Exactly how rotational symmetry affects the H-polarized band structures can be elucidated by modeling wave scattering within the hollow oval rods. Light with a long wavelength cannot easily be trapped or resonate in the rods; hence, the interaction between the fields of the rods must be considered to examine the H1 gap. In the H-polarization modes, the fields are oriented in the plane and are distributed among the rod and air regions satifying the continuity condition. The air-space size between the rods remains constant under inner-rod rotation through an arbitrary angle, indicating that the interaction between the fields of the rods affects the H-polarization bands in almost the same way at all angles of rotation, slightly changing the H1 gap width. Under whole-rod rotation, the variation in the air-space size influences the wave scattering between rods, so the H1 gap width varies markedly.

Figures 5.11 (c) and (d) plot the H3 gap width for inner and whole rod rotations, respectively. As shown in the diagrams, the gap width associated with the inner–rod rotation increases with the rotating angle, but that associated with the whole-rod rotation approaches to zero at around $\theta_1 = \theta_2 = 40°$. Light with a short wavelength propagating in the rod may cause resonance and be trapped in the cavity, so the H3 gap width depends strongly on the shape of the rods. The shape of the hollow oval rod is changed for the inner-rod rotation, so the H3 gap width varies because the structural symmetry is broken. The shape of the rods is constant under whole-rod rotation to an arbitrary angle, so the H3 gap width varies markedly because the rotational symmetry is broken. The results associated with the inner-rod rotation are governed mainly by the shape of the rod, and those associated with the whole-rod

rotation are governed by the angle of rotation.

The E-polarization modes of the hollow oval structure under inner-rod or whole-rod rotation exhibit many flat-band gaps. Figures 5.12(a) and (b) show plots of the E-polarization gap width vs. the angles of inner-rod and whole-rod rotations, respectively. As the diagram shows, the E-polarization gap widths vary markedly under inner-rod rotation. The E1 (between the 7th and 8th bands) and E2 (between the 7th and 8th bands) gap widths at $\alpha_1 = \alpha_2 = 1.6$ as a function of rotating angle is plotted in Fig. 5.13. The gap widths in E1 and E2 vary slightly with the rotation of the whole rod, but vary markedly with the rotation of the inner rod. These results may also be understood by considering the field distribution within the hollow oval rods.

Figure 5.14(a) shows the field patterns of the structure at $0°$, and Figs. 5.14(b) and 5.14(c) show those of the inner-rotation and whole-rotation structures at $30°$, respectively. The E-polarization mode is associated with the displacement field D normal to the plane, $D(\vec{r}) = d(\vec{r})\hat{e}_z$, where $d(\vec{r})$ is a scalar function. The field patterns in each figure are displayed for the seventh band at the *K*-symmetry point. The profiles of the rods are shown as solid lines, and the brightness represents the amplitude of the displacement field. The rotational symmetry is broken by rotating whole rods, but the amplitude of the displacement field, the field distribution and the amount of field energy in the dielectric regions are equal to those in Fig. 5.14(a). This result may imply that the E-polarization modes are confined within hollow rods, and the band structure then exhibits the flat-band property. The confinement in the E-polarization mode may be attributed to the high contrast between refractive indices in the extraordinary direction, so the line shape of the band is invariable and the frequency varies slightly.

Moreover, the field energy associated with inner-rod rotation is similar to that in

Fig. 5.14(b), but the field distributions differ. The fields inside the rods tend to move toward the thin dielectric region, and the fields in the thin region are expelled from the dielectric region. Consequently, the proportion of fields inside the rods varies under inner-rod rotation, strongly influencing the E-polarization band structures. The field patterns of the higher bands at an arbitrary angle of rotation have also been calculated, and the results and discussions are analogous to those mentioned above. Therefore, the E-polarization band structures are determined primarily by the shapes of the individual rods, even though the rotational symmetry of hollow oval structures is broken.

Overlapping the band gaps of H- and E-polarization modes gives the complete band gap. Figures 5.15(a) and (b) show plots of the complete gap widths vs. the angles of inner-rod and whole-rod rotations, respectively. The results reveal that the E-polarization modes dominate the complete PBG width under inner-rod rotation and the H-polarization modes dominate the complete PBG width under whole-rod rotation. The complete gap widths of the inner-rod rotation vary markedly because they are governed by the E-polarization modes. The complete gap widths under whole-rod rotation decline as the angle of rotation increases because they are dominated by the H-polarization modes. The properties of the formed complete PBGs also have the same results for any $\alpha_1 (= \alpha_2)$ value.

The photonic crystals considered here are made of 2-dimensional array of tellurium hollow oval rods. i.e., the light wave is free along the direction of rods. To approach to the case, the height of the rods should be infinity or much larger than the lattice constant of the 2D crystalline arrays. Practically and macroscopically, if the height of the rods is an order larger than the beam size of perpendicular (to the rods) incident light, which can be minimized to a few wavelengths, the height of rods can then be considered as infinity ideally. Microscopically, for the case of perpendicular

incidence to the rods, if the height of the rods is an order larger than the light wavelength, the wave phenomena of light can be neglected along the direction of rods and the height of rods can be considered infinity. So for the structures we considered here, the minimal height of the rods should be larger than tens microns to ensure our calculation results well agree with the results for the exact 2D array photonic crystals. For the smaller height of the rods, our analysis and comments would be more or less applicable or valid until the photonic crystals become critically 3D confined systems.

With the current semiconductor nano-lithographic technology, it would not be very difficult to pattern the hollow rods with cross section in the size of micrometers. However, tellurium is not a popular material in the nano-lithographic technology; it is still not well developed for making Te microstructures to photonic crystals. The most challenging task could be the process for etching the Te bulk to long rods.

In this chapter, the plane-wave method is used to calculate the field patterns and the band structure of a triangular lattice of hollow Te rods. Firstly, three deformed structures are designed by altering the geometric parameters of rods to investigate the effect of structural symmetry on E- and H-polarization modes. The results in the H-polarization modes indicate that the air space among the rods dominates the low-frequency gaps while the shape of the rods affects mainly the high-frequency gaps. The results in the E-polarization modes indicate a strong relationship between the shape of the rods and the band gaps, as determined from the field patterns. Two rotations, inner and whole rod rotations, are considered with fixed geometric parameters to investigate the effect of rotational symmetry on E- and H-polarization modes. The effect on the E-polarization mode for rotational structures is similar to that for deformed structures. However, H-polarization modes are affected not only by the field distribution among rods but also by the reduction of rotational symmetry. Analyzing the structural and rotational symmetry of the hollow structure is useful in

understanding the properties of the formed PBGs and provides a path for designing proper photonic crystal structures with desired PBGs.

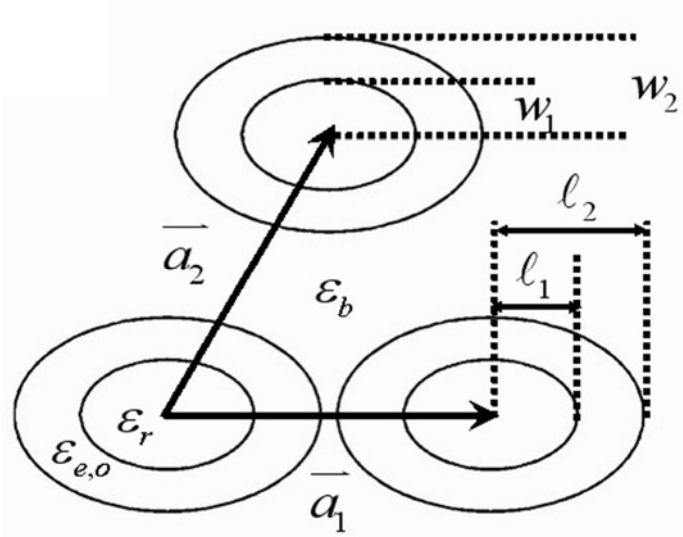

Figure 5.1 Schematic configuration of a triangular lattice with hollow oval Te rods.

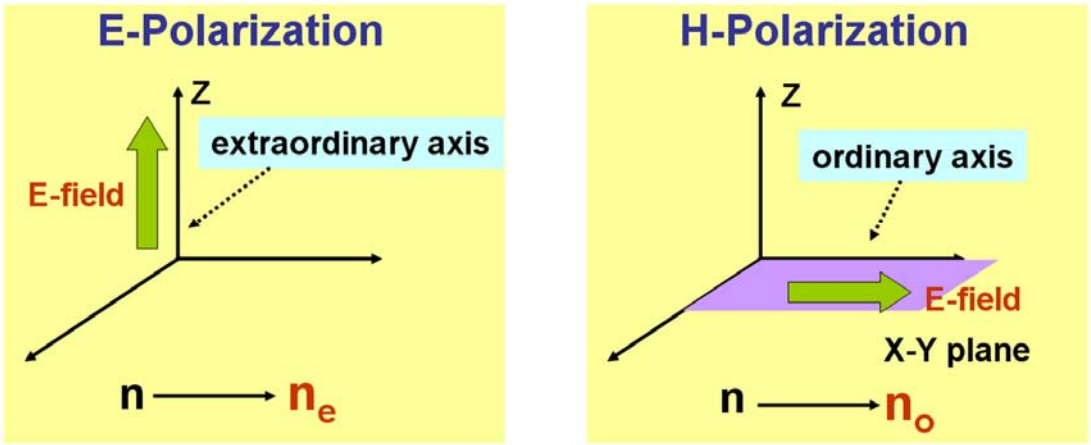

Figure 5.2 The representation of anisotropic optical property. The refractive index is n_e when the electric field vector in the E-polarization mode is parallel to the extraordinary axis, while the refractive index is n_0 when the electric field vector in the H-polarization mode is perpendicular to the extraordinary axis.

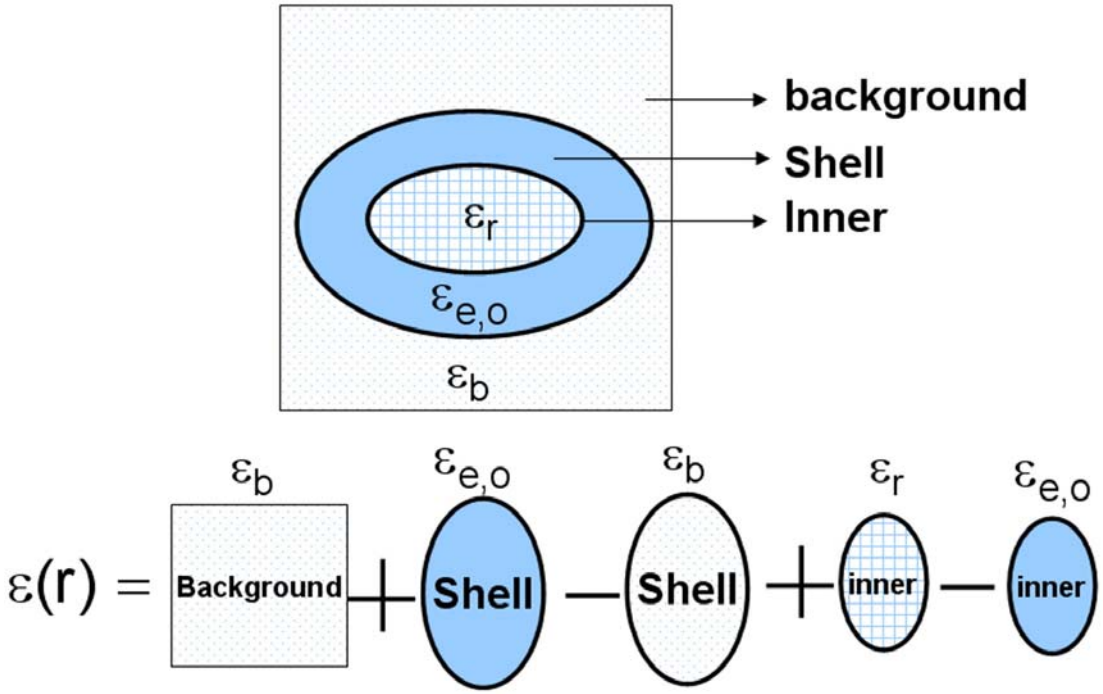

Figure 5.3 Schematic illustration of the unit cell construction for the hollow oval dielectric rod. The dielectric function can be understood from this illustration.

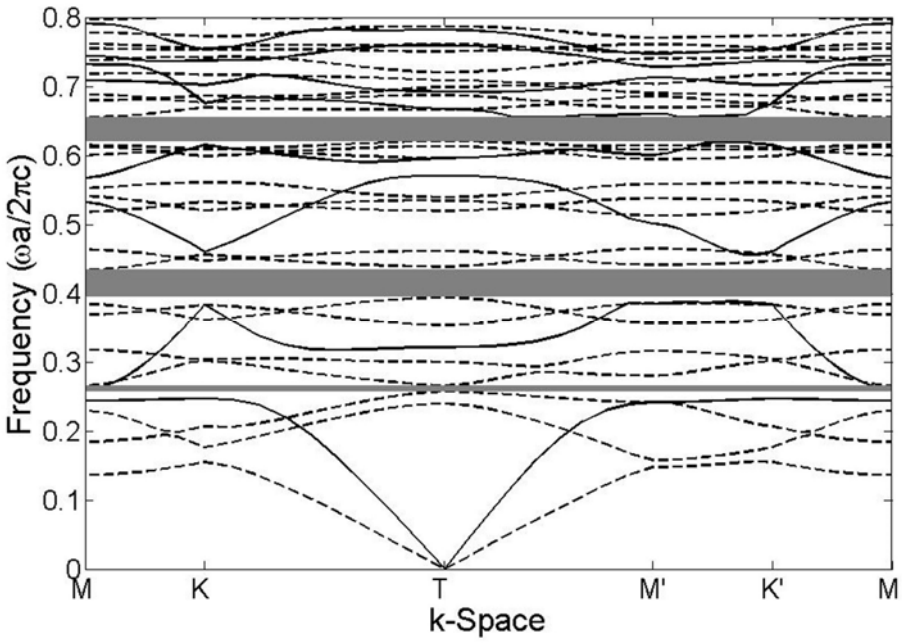

Figure 5.4 The band structure for a triangular lattice of hollow oval rods at a rotation angle of $\theta_1 = \theta_2 = 0°$. The geometric parameters (ℓ_1, ℓ_2, α) for hollow oval rods are taken as $\ell_1 = 0.27\,a$, $\ell_2 = 0.48\,a$, and $\alpha = 1.58$.

Table 1. Complete photonic band gap widths in unit $\omega a/2\pi c$ for a photonic crystal with various refractive indices.

	n_o=4.78	4.79	4.80	4.81	4.82
n_e=6.18	Gap1: 0.0520 Gap2: 0.0347	Gap1: 0.0520 Gap2: 0.0347	Gap1: 0.0520 Gap2: 0.0338	Gap1: 0.0520 Gap2: 0.0295	Gap1: 0.0520 Gap2: 0.0252
6.19	Gap1: 0.0517 Gap2: 0.0346	Gap1: 0.0517 Gap2: 0.0346	Gap1: 0.0517 Gap2: 0.0346	Gap1: 0.0517 Gap2: 0.0355	Gap1: 0.0517 Gap2: 0.0322
6.20	Gap1: 0.0513 Gap2: 0.0325	Gap1: 0.0513 Gap2: 0.0376	Gap1: 0.0513 Gap2: 0.0346	Gap1: 0.0513 Gap2: 0.0346	Gap1: 0.0515 Gap2: 0.0372
6.21	Gap1: 0.0510 Gap2: 0.0266	Gap1: 0.0510 Gap2: 0.0317	Gap1: 0.0510 Gap2: 0.0345	Gap1: 0.0510 Gap2: 0.0377	Gap1: 0.0510 Gap2: 0.0345
6.22	Gap1: 0.0507 Gap2: 0.0208	Gap1: 0.0507 Gap2: 0.0259	Gap1: 0.0507 Gap2: 0.0309	Gap1: 0.0507 Gap2: 0.0344	Gap1: 0.0507 Gap2: 0.0344

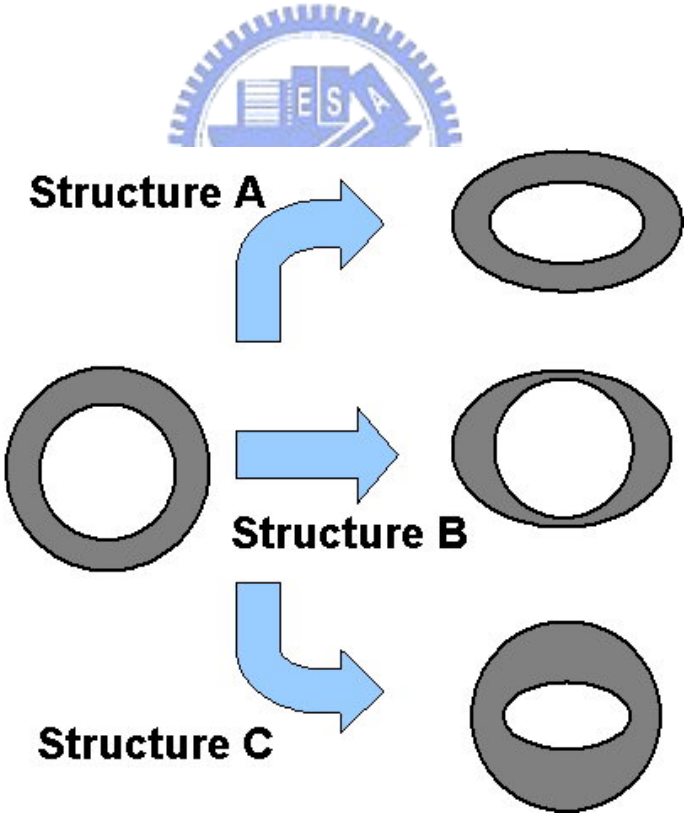

Figure 5.5 The Schematic diagrams of three deformed hollow structures. The structures are deformed by altering the factors α_1 and α_2.

Table 2. Complete photonic band gaps width, in unit of $\omega a/2\pi c$, of photonic crystals with constant refractive indices $(n_e = 6.2, n_o = 4.8)$ and various *L*1 and L2 lengths in unit of the lattice constant.

	L2=0.48*(1-10%)	0.48*(1-5%)	0.48	0.48*(1+5%)	0.48*(1+10%)
L1= 0.27*(1-10%)	Gap1: 0.0502 Gap2: 0.0305	Gap1: 0.0534 Gap2: 0.0259	Gap1: 0.0429 Gap2: 0.0204	Gap1: 0.0248 Gap2: 0.0138	Gap1: 0 Gap2: 0.0152
0.27*(1-5%)	Gap1: 0.068 Gap2: 0	Gap1: 0.0512 Gap2: 0.0267	Gap1: 0.0410 Gap2: 0.0257	Gap1: 0.0232 Gap2: 0	Gap1: 0 Gap2 : 0.0149
0.27	Gap1: 0.0707 Gap2: 0	Gap1: 0.057 Gap2: 0.029	Gap1: 0.0510 Gap2: 0.0377	Gap1: 0.0237 Gap2: 0.0123	Gap1: 0 Gap2: 0
0.27*(1+5%)	Gap1: 0.0693 Gap2: 0	Gap1: 0.0584 Gap2: 0	Gap1: 0.0412 Gap2: 0.0134	Gap1: 0.0198 Gap2: 0.0073	Gap1: 0 Gap2: 0
0.27*(1+10%)	Gap1: 0.0664 Gap2: 0	Gap1: 0.0573 Gap2: 0	Gap1: 0.0412 Gap2: 0	Gap1: 0.0210 Gap2: 0.0161	Gap1: 0.0084 Gap2: 0

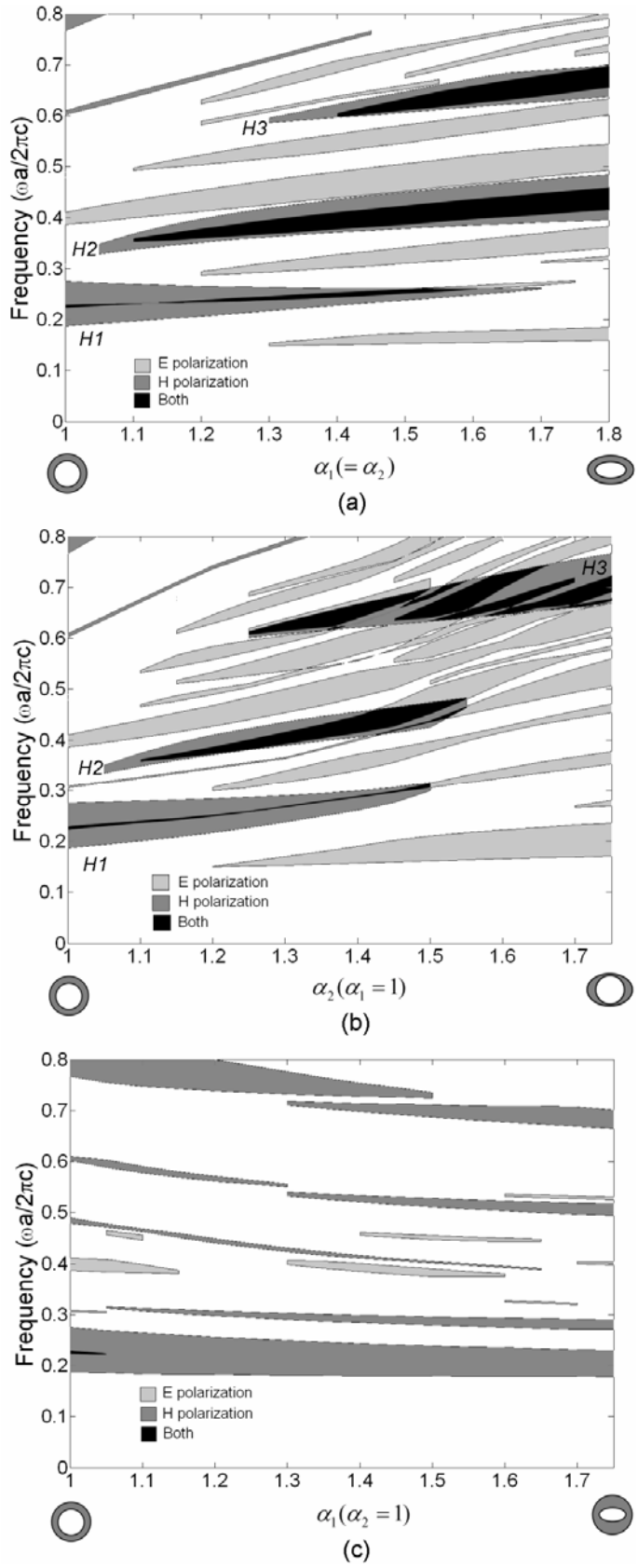

Figure 5.6 Gap maps of the (a) structure A, $\alpha_1 = \alpha_2$ (b) structure B, $\alpha_1 = 1$, and (c) structure C, $\alpha_2 = 1$. The major-axis lengths of shell and inner rods are fixed to $\ell_1 = 0.27a$ and $\ell_2 = 0.48a$.

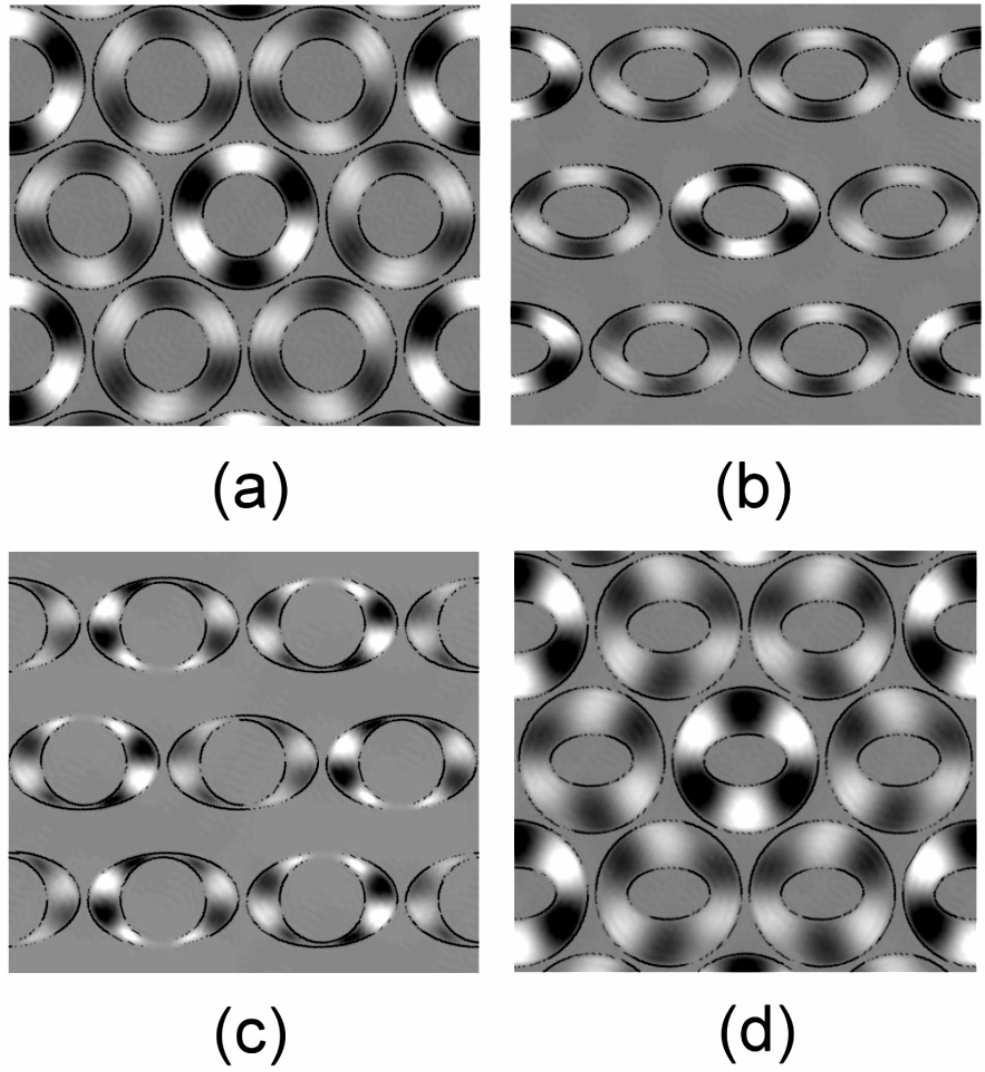

Figure 5.7 Displacement-field distribution of E-polarization modes inside the hollow rods in the (a) hollow circular structure, $\alpha_1 = \alpha_2 = 1$ (b) structure A with $\alpha_1 = \alpha_2 = 1.6$ (c) structure B with $\alpha_1 = 1,\ \alpha_2 = 1.6$, and (d) structure C with $\alpha_1 = 1.6,\ \alpha_2 = 1$ at K -symmetry point.

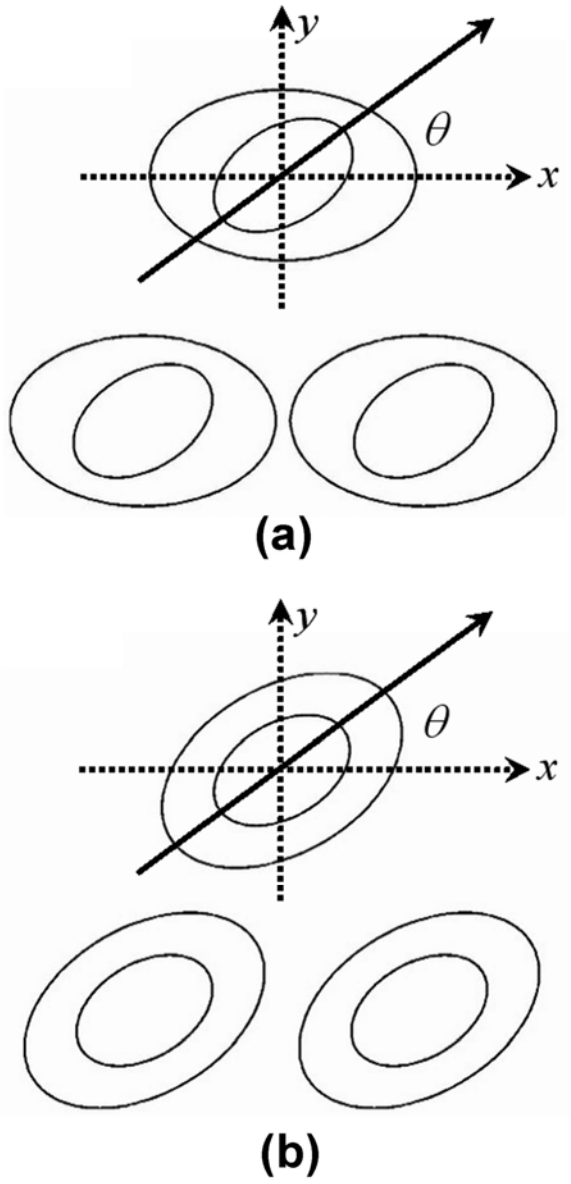

Figure 5.8 Schematic configuration of triangular lattice with hollow oval Te rods. The inner rod rotates at an angle of θ_1. The outer shell rotates at an angle of θ_2. (a) inner-rod rotation: $\theta_1 = \theta$ and $\theta_2 = 0^\circ$, and (b) whole-rod rotation: $\theta_1 = \theta_2 = \theta$.

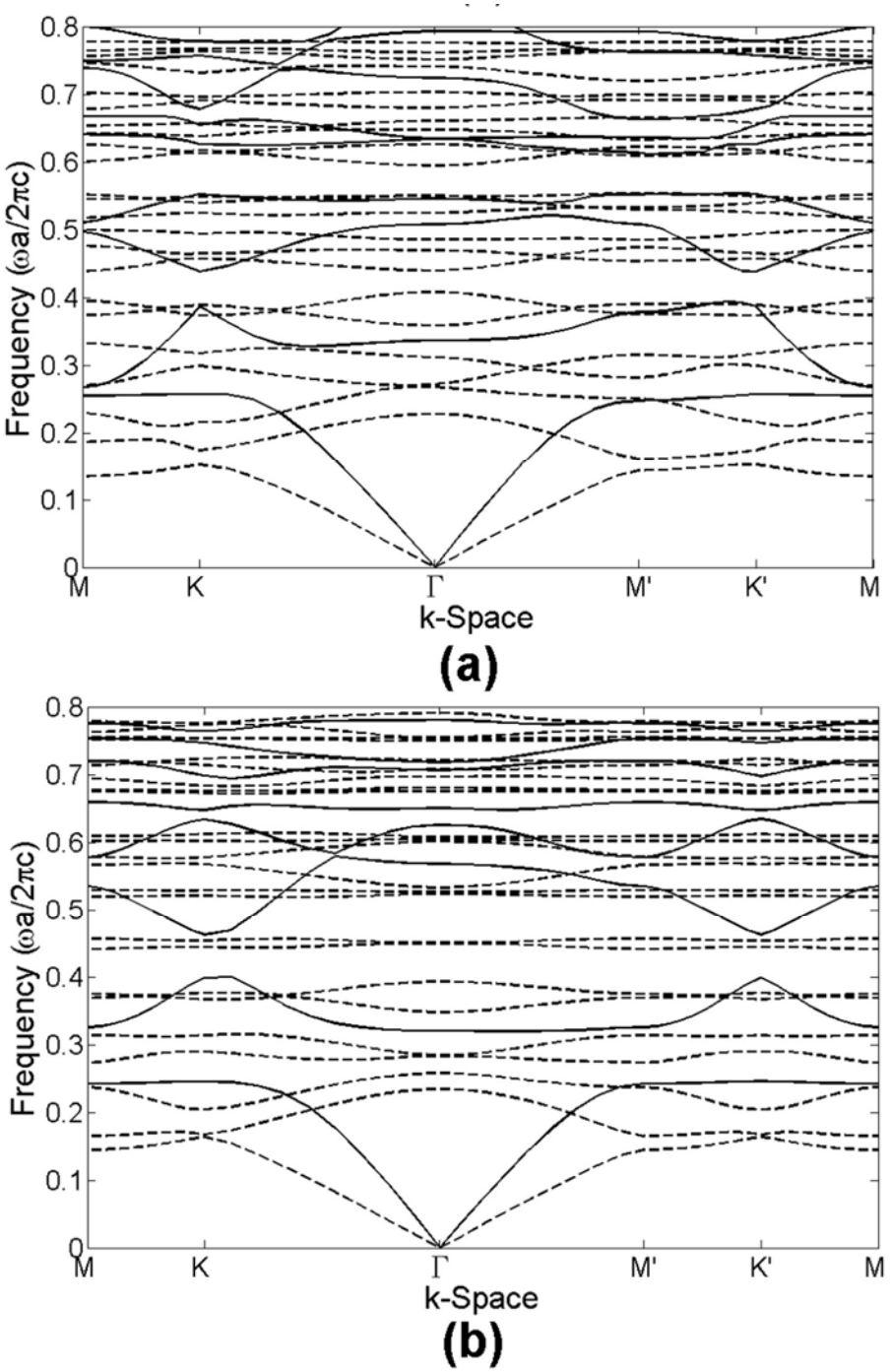

Figure 5.9 Photonic band structures for (a) inner-rod rotation with $\theta_1 = 30^\circ$ and $\theta_2 = 0^\circ$, and (b) whole rod-rotation with $\theta_1 = \theta_2 = 30^\circ$.

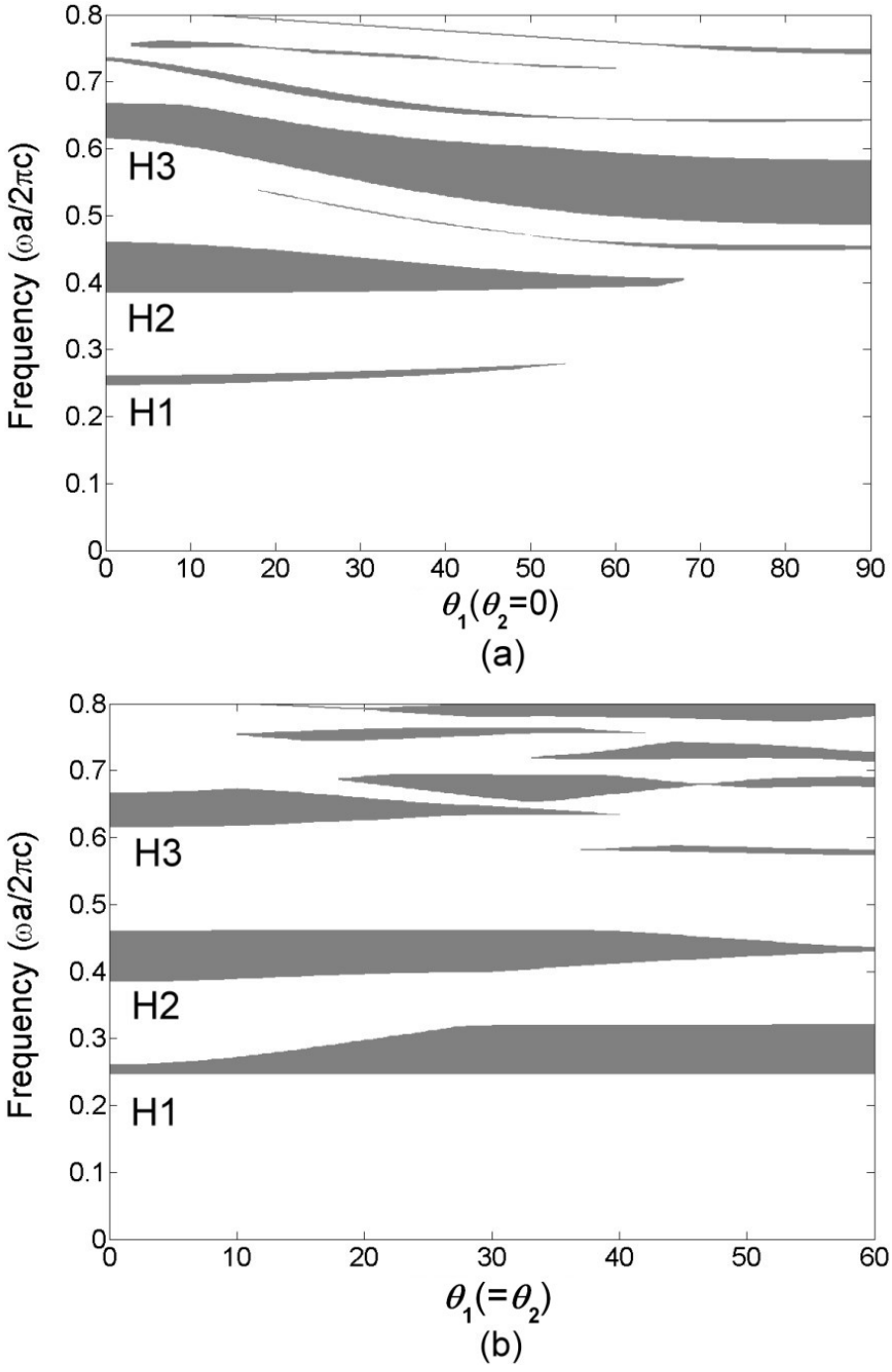

Figure 5.10 H-polarization band gap as function of rotation angle for (a) inner-rod rotation with $\theta_2 = 0^\circ$ and (b) whole-rod rotation with $\theta_1 = \theta_2$.

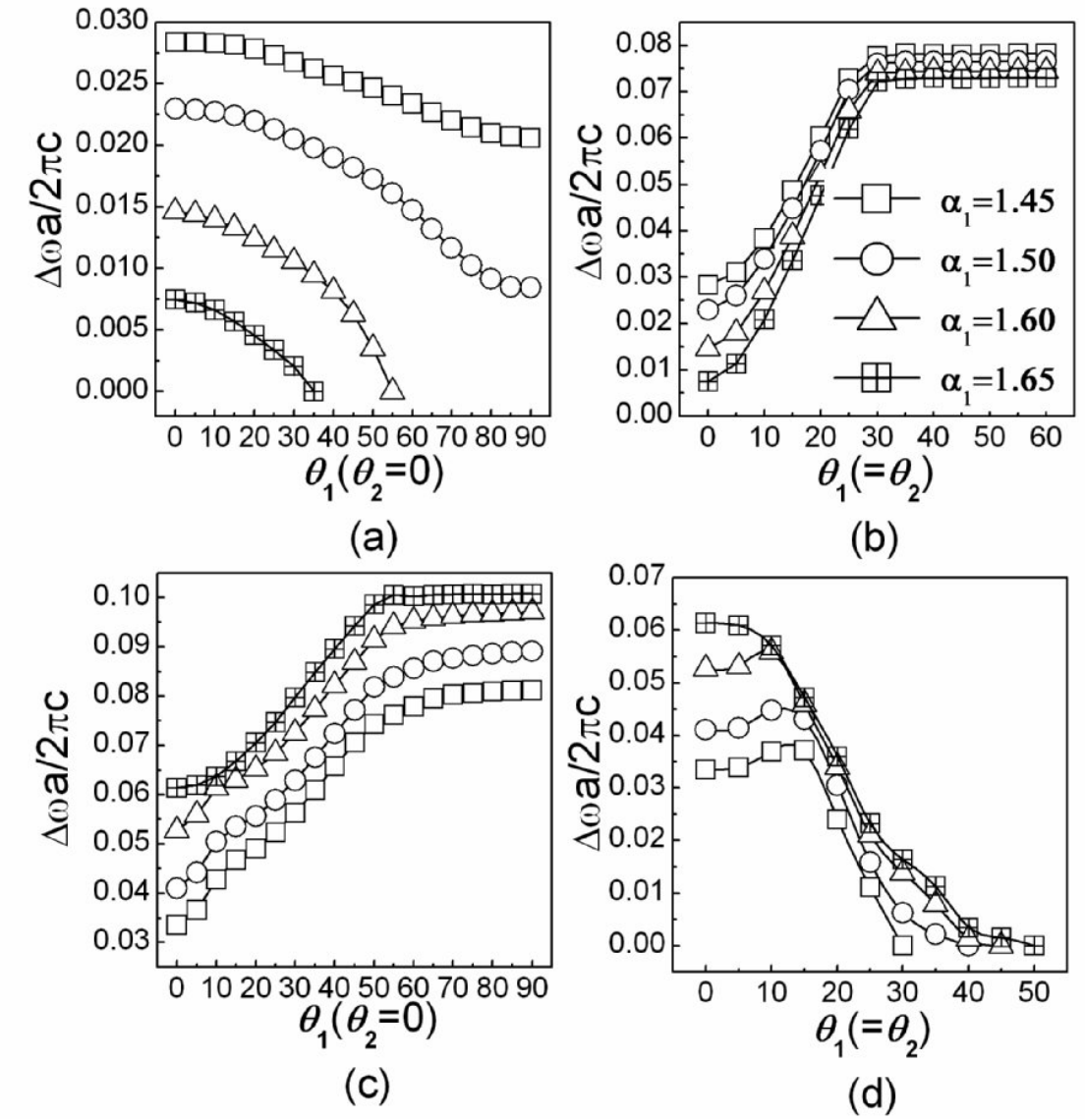

Figure 5.11 Gap widths as a function of rotating angles θ_1 and θ_2 for inner rod and whole rod rotations with various $\alpha_1(=\alpha_2)$. H1 gap width for (a) inner rod rotations, $\theta_2 = 0$, and (b) whole rod rotations, $\theta_2 = \theta_1$; H3 gap width for (c) inner rod rotations, $\theta_2 = 0$, and (d) whole rod rotations, $\theta_2 = \theta_1$. Each curve in the same line style in (a), (c), and (d) corresponds to the same quantity of α_1, as the list inserted in (b).

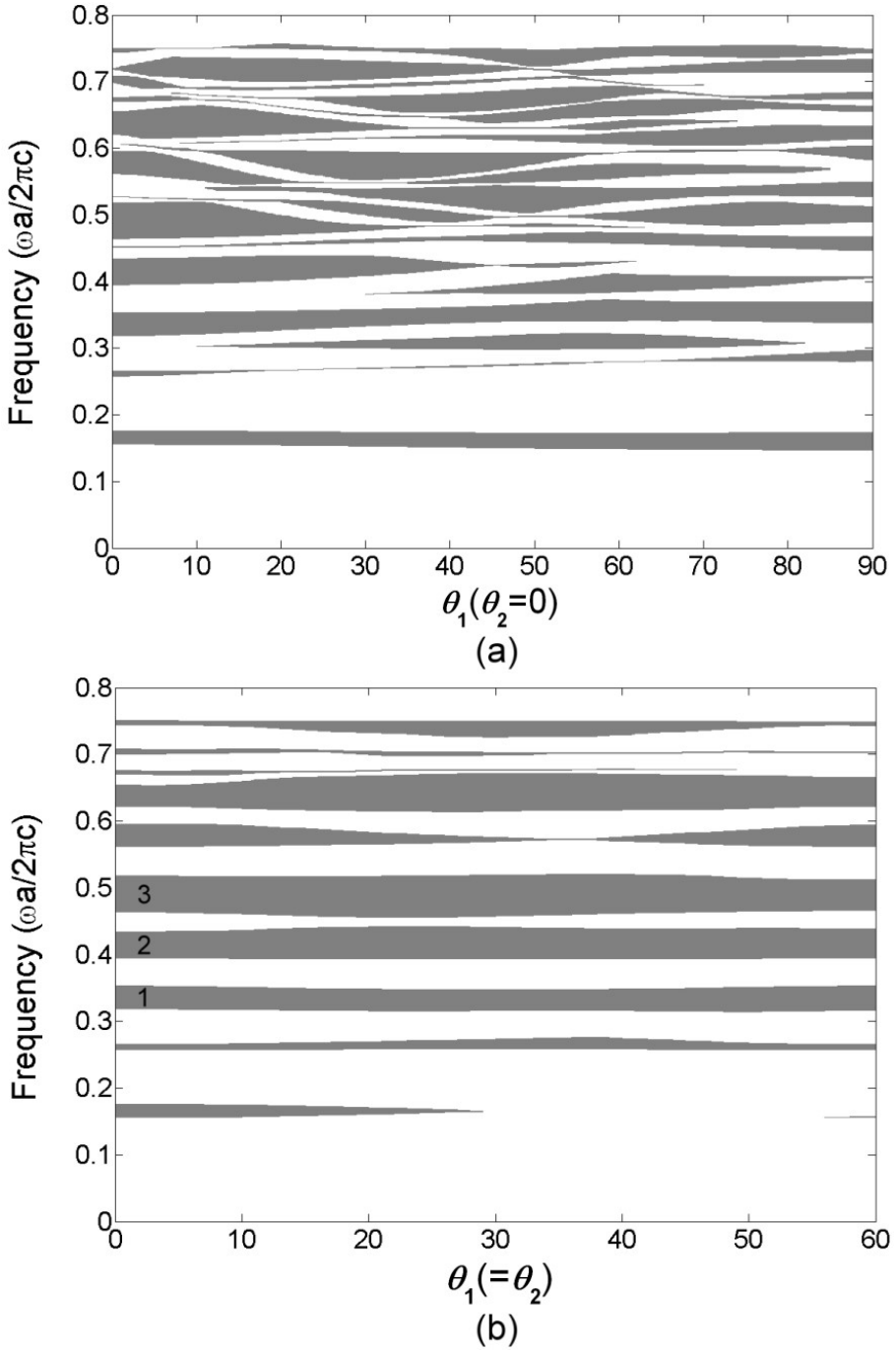

Figure 5.12 E-polarization band gap as function of rotation angle for (a) inner-rod rotation with $\theta_2 = 0^\circ$ and (b) whole-rod rotation with $\theta_1 = \theta_2$.

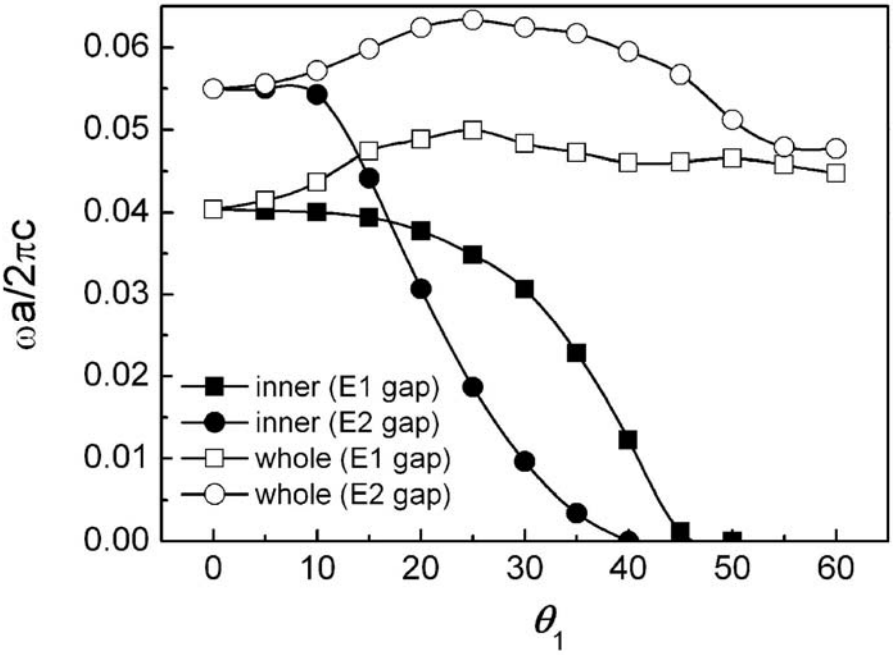

Figure 5.13 E1 and E2 gap widths as a function of rotating angle θ_1 for inner rod and whole rod rotations at $\alpha_1 = \alpha_2 = 1.6$.

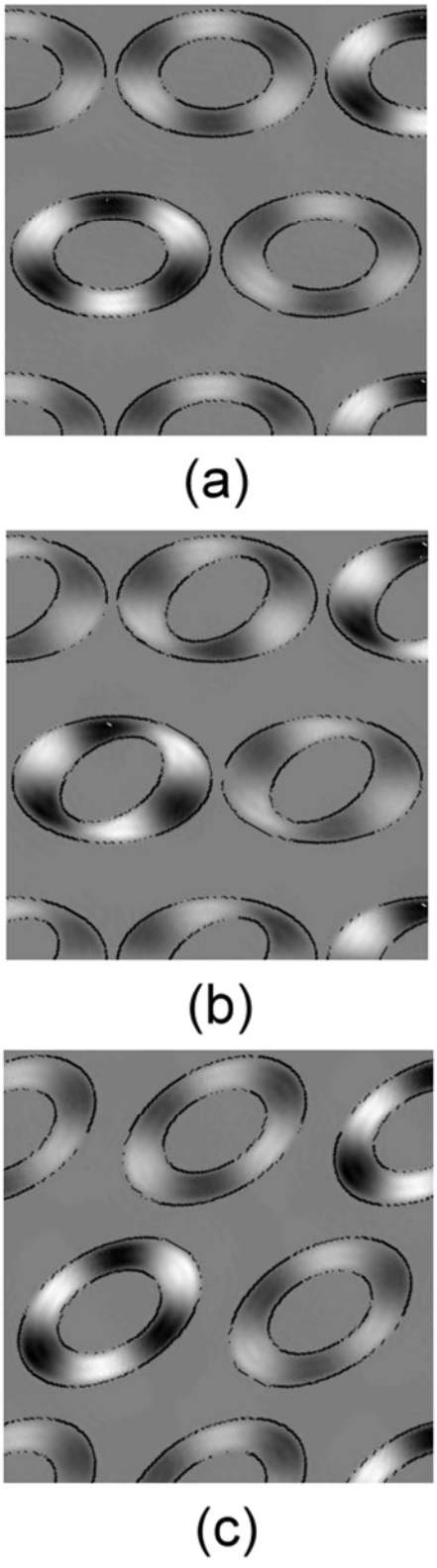

Figure 5.14 Field patterns of E-polarization modes inside hollow oval rods for (a) $\theta_1 = \theta_2 = 0^\circ$, (b) inner-rod rotation with $\theta_1 = 30^\circ$ and $\theta_2 = 0^\circ$, and (c) whole-rod rotation with $\theta_1 = \theta_2 = 30^\circ$ at K-symmetry point.

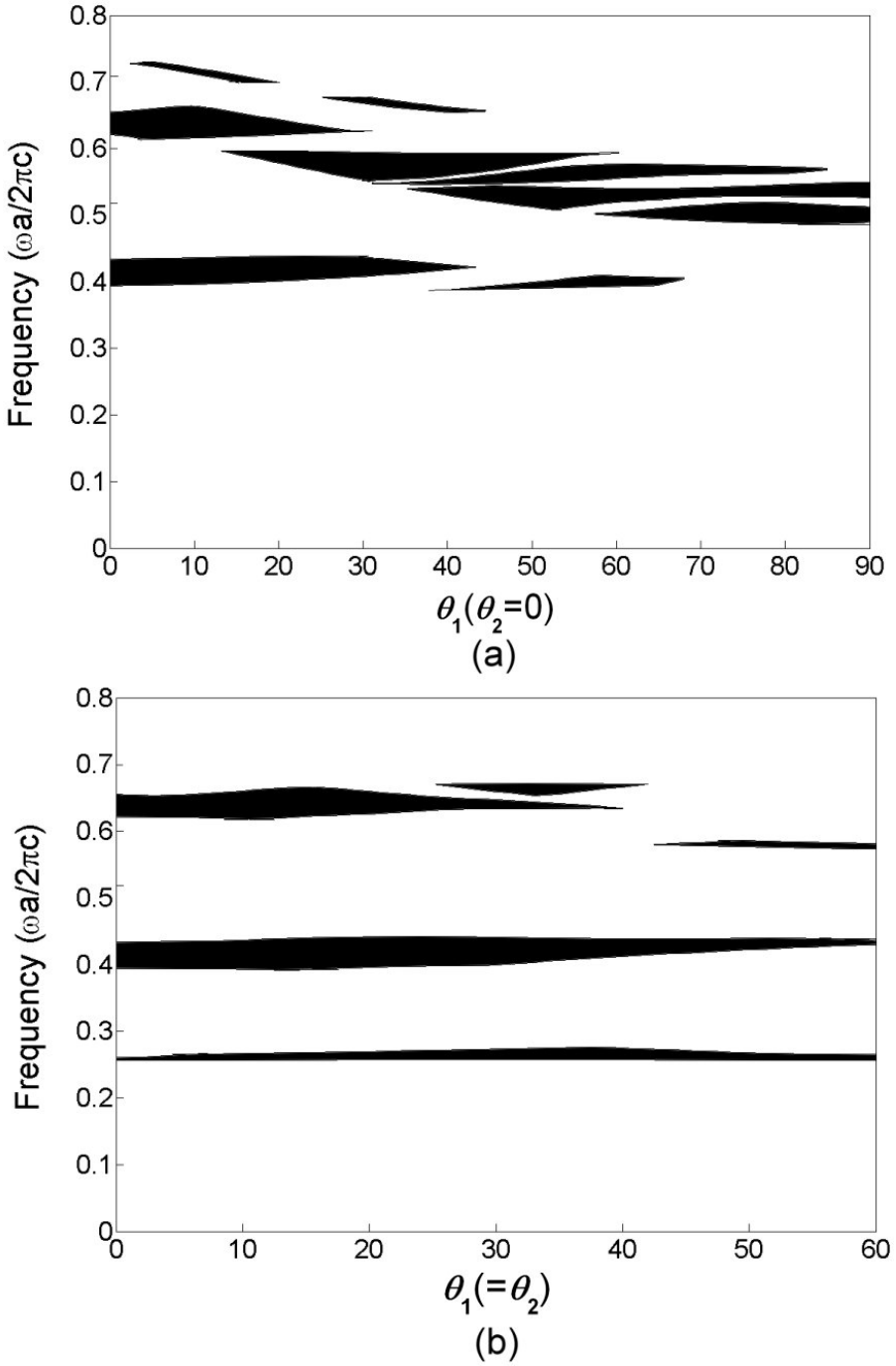

Figure 5.15 Complete photonic band gap as function of rotation angle θ_1 for (a) inner-rod rotation with $\theta_2 = 0^\circ$ and (b) whole-rod rotation with $\theta_1 = \theta_2$.